Cloud-resolving simulation of TOGA-COARE using parameterized large-scale dynamics

Shuguang Wang,[1] Adam H. Sobel,[2] and Zhiming Kuang[3]

Received 26 November 2012; revised 17 May 2013; accepted 20 May 2013.

[1] Variations in deep convective activity during the 4 month Tropical Ocean Global Atmosphere-Coupled Ocean Atmosphere Response Experiment (TOGA-COARE) field campaign are simulated using a cloud-resolving model (CRM). Convection in the model is coupled to large-scale vertical velocities that are parameterized using one of two different methods: the damped gravity wave (Damped-wave) method and the weak temperature gradient (WTG) method. The reference temperature profiles against which temperature anomalies are computed are taken either from observations or from a model integration with no large-scale vertical motion (but other forcings taken from observations); the parameterized large-scale vertical velocities are coupled to those temperature (or virtual temperature) anomalies. Sea surface temperature, radiative fluxes, and relaxation of the horizontal mean horizontal wind field are also imposed. Simulations with large-scale vertical velocity imposed from the observations are performed for reference. The primary finding is that the CRM with parameterized large-scale vertical motion can capture the intraseasonal variations in rainfall to some degree. Experiments in which one of several observation-derived forcings is set to its time-mean value suggest that those which influence direct forcings on the moist static energy budget—surface wind speed and sea surface temperature (which together influence surface evaporation) and radiative cooling—play the most important roles in controlling convection, particularly when the Damped-wave method is used. The parameterized large-scale vertical velocity has a vertical profile that is too bottom-heavy compared to observations when the Damped-wave method is used with vertically uniform Rayleigh damping on horizontal wind, but is too top-heavy when the WTG method is used.

Citation: Wang, S., A. H. Sobel, and Z. Kuang (2013), Cloud-resolving simulation of TOGA-COARE using parameterized large-scale dynamics, *J. Geophys. Res. Atmos.*, *118*, doi:10.1002/jgrd.50510.

1. Introduction

[2] Cloud-resolving models (CRMs) on small doubly periodic domains have been widely used to study many aspects of deep convection and its response to the large-scale environment. One important application of CRMs is to simulate specific sequences of weather events which have been observed in field campaigns [e.g., *Soong and Ogura*, 1980, *Grabowski et al.*, 1996, *Johnson et al.*, 2002, *Tao et al.*, 2004; *Khairoutdinov and Randall*, 2003; *Blossey et al.*, 2007; *Fridlind et al.*, 2012]. In this context, it is standard to specify large-scale forcings derived from sounding arrays. These forcings—particularly the large-scale vertical motion or vertical advection terms—control the occurrence and intensity of convection and keep it close to that observed. The simulated precipitation, in particular, is tightly constrained by the forcings. Significant model biases may appear in the simulated temperature, moisture, clouds, and radiative and surface fluxes, but not in precipitation.

[3] While much has been learned from such simulations, it may be argued that they misrepresent the causality of many tropical circulations. Large-scale vertical motion is arguably as much a consequence of deep convection as a cause [e.g., *Mapes*, 1997; *Sobel and Bretherton*, 2000]. When large-scale vertical motion is specified, one cannot use the simulation to understand the factors that control the occurrence or intensity of deep convection.

[4] In the past decade, methods have been developed to allow interaction between CRM-resolved convective dynamics and parameterized large-scale dynamics. One group of methods uses the weak temperature gradient (WTG) approximation [e.g., *Sobel and Bretherton*, 2000; *Raymond and Zeng*, 2005]. Another set of methods involves coupling to a large-scale gravity wave of specified horizontal wavelength [*Kuang*, 2008, 2011; *Blossey et al.*, 2009; *Romps*, 2012a, 2012b]. We explore both of these in this study. Still others

[1]Department of Applied Physics and Applied Mathematics, Columbia University, New York, New York, USA.
[2]Department of Applied Physics and Applied Mathematics, Department of Earth and Environmental Sciences, and Lamont-Doherty Earth Observatory, Columbia University, New York, New York, USA.
[3]Department of Earth and Planetary Sciences and School of Engineering and Applied Sciences, Harvard University, Cambridge, Massachusetts, USA.

Corresponding author: S. Wang, Department of Applied Physics and Applied Mathematics, Columbia University, New York, NY 10027, USA. (sw2526@columbia.edu)

2169-897X/13/10.1002/jgrd.50510

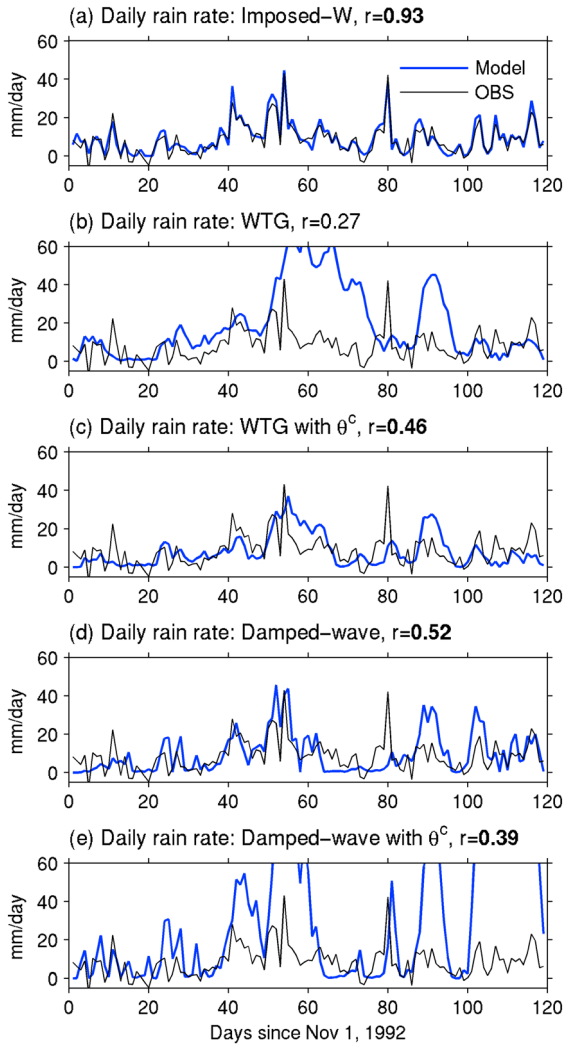

Figure 1. Budget-derived daily rainfall (black) and model-simulated rainfall (blue) for (a) the Imposed-W experiment, (b) the WTG experiment, (c) as Figure 1b but with a correction θ^c to the target temperature profile so that its time mean equals that from an experiment with no large-scale circulation, (d) the Damped-wave experiment, (e) as Figure 1b but with θ^c. Bold values of correlation coefficient, r, indicate that it is statistically significant at the 95% level.

have been introduced but are not considered here [e.g., *Bergman and Sardeshmukh*, 2004; *Mapes*, 2004].

[5] Thus far, these parameterizations of large-scale dynamics have been used almost exclusively in idealized settings. They have been used to study, for example, the response of deep convection to relative sea surface temperature [*Sobel and Bretherton*, 2000; *Wang and Sobel*, 2011; *Kuang*, 2012], or imposed surface wind speed [*Raymond and Zeng*, 2005; *Sessions et al*., 2010], or the interaction of convection with a pure plane gravity wave [*Kuang*, 2008], or idealized tropical depression [*Raymond and Sessions*, 2007]

[6] In this study, we use these methods to simulate specific time-varying field observations. We expect that these methods will not be able to simulate the variations of deep convection as accurately as the standard method with specified forcing can, because the large-scale vertical motion is no longer directly constrained by observations. On the other hand, the degree to which these variations are simulated represents genuine success or failure of the simulation. To the extent that the simulations are successful, the model can be used to obtain nontrivial information about what factors control the convection.

[7] We use a CRM with parameterized large-scale dynamics to simulate a 4 month sequence of weather observed in the western Pacific Ocean during the TOGA-COARE (Tropical Ocean Global Atmosphere-Coupled Ocean Atmosphere Response Experiment [*Webster and Lukas*, 1992]) field program. The atmospheric state was sampled by a sounding array during the 4 month intensive observing period, from 1 November 1992 to 28 February 1993. During this time, two active phases of the Madden-Julian oscillation (MJO) traversed the sounding array [*Chen et al*., 1996]. Several previous studies have reported CRM and SCM (single column model) simulations of the MJO during TOGA-COARE, using standard methods with imposed large-scale vertical motion or vertical advection [e.g., *Emanuel and Živković-Rothman*, 1999; *Johnson et al*., 2002; *Wu et al*., 1998]. Here, our focus will be on capturing the evolution of convection over intraseasonal time scales during the entire TOGA-COARE period using parameterized large-scale dynamics. To the extent that we are able to simulate the time variations of precipitation, the implication is that the processes which are specified from observations as time-varying forcings—which no longer include large-scale vertical motion—control the variations in deep convection.

2. Data, Method, and Numerical Method

2.1. Large-Scale Forcing Data

[8] We use version 2.1 of the large-scale forcings derived from the Intensive Flux Array (IFA) sounding network [*Ciesielski et al*., 2003] from 1 November 1992 to 28 February 1993 during the TOGA-COARE. After a long suppressed phase of the MJO, the first active period of convection began around day 40 and ended around day 55 from 1 November, as shown in black in Figure 1a. The second active MJO phase passed the COARE region during the interval from day 80 to the end of the simulated period.

2.2. Numerical Model

[9] We use the WRF model version 3.3 [*Skamarock et al*., 2008]. Boundary layer turbulence and vertical transport by subgrid eddies are parameterized using the Yonsei University scheme [*Hong et al*., 2006]; horizontal transport by subgrid eddies is treated using Smagorinsky first-order closure; the surface moisture and heat fluxes are parameterized following Monin-Obukhov similarity theory; the radiative transfer scheme is from the Community Atmosphere Model [*Collins et al*., 2004]; and the Purdue-Lin scheme is used for cloud microphysics [*Lin et al*., 1983]. The horizontal and vertical advection schemes are fifth-order and third-order accurate, respectively. Moisture and condensate are advected using a positive definite scheme. We use the implicit damping scheme to suppress unphysical reflection of vertically propagating gravity waves in the top 5 km of the numerical grid [*Klemp et al*., 2008]. We use a doubly periodic domain with zero Coriolis parameter. Sixty vertical levels are used

with stretched vertical level spacing. The horizontal grid spacing is 1 km within a grid of $64 \times 64 \times 22\,\mathrm{km}^3$. An adaptive time step is used for all simulations in this study.

2.3. Methodology

[10] As a point of reference, we first impose the following forcings to our CRM at 6-hourly resolution, as in many previous studies: (1) large-scale vertical motion to advect domain-averaged potential temperature and moisture, (2) horizontal advective tendencies of moisture and temperature, (3) time-varying uniform sea surface temperature (SST) as the lower boundary condition, and (4) relaxation of the horizontal domain mean horizontal winds to the observed IFA mean profiles with a relaxation time scale of 1 h.

[11] Of these forcings, large-scale vertical velocity is by far the most important for controlling surface rainfall. Horizontal advection terms are included in the above reference simulation, but not in the simulations with parameterized large-scale dynamics.

[12] Horizontal advection can be treated in a number of ways: the horizontal advection term—dot product of a large-scale horizontal velocity with a large-scale horizontal moisture gradient—can be imposed directly (as is typically done in simulations with imposed large-scale vertical motion or vertical advection); one can parameterize the horizontal advection term by applying a specified relaxation of the horizontally averaged moisture profile in the CRM toward a reference profile of moisture, representing advection by a specified rotational large-scale velocity on a specified length scale [e.g., *Sobel and Bellon*, 2009; *Wang and Sobel*, 2012]; or one can parameterize the advection as "lateral entrainment," as defined in *Raymond and Zeng* [2005], representing the drawing of the reference profile air into the CRM domain by a divergent horizontal velocity diagnosed from the vertical WTG mass flux.

[13] Contrasting results with and without horizontal advection terms in our reference simulations suggests that their impact is small for surface rainfall for the reference simulation (not shown), and their proper inclusion in simulations with parameterized large-scale dynamics is a subtle matter. Including them as fixed forcings neglects their actual dependence on the local state and can allow bad behavior if the model is biased (for example, if the advective forcing on humidity is negative and the humidity becomes zero, there is nothing to prevent it from becoming negative). We have represented horizontal moisture advection as a relaxation to an upstream value in idealized studies [e.g., *Sobel and Bellon*, 2009; *Wang and Sobel*, 2012], but determining the appropriate upstream value and relaxation time is more complex in the present observation-based case studies. The lateral entrainment approach neglects advection by the rotational flow, which is often larger than the divergent component. Because of these limitations, we defer inclusion of horizontal advection to future work, while acknowledging its potential importance for tropical intraseasonal variability.

[14] We have used both the WTG and damped gravity wave methods to parameterize large-scale dynamics. In both methods, large-scale vertical motion is dynamically derived as part of the model solution and used for advecting domain-averaged temperature and moisture in the vertical. In the WTG method, large-scale vertical velocity W in the free troposphere is derived as follows:

$$W\frac{\partial\theta}{\partial z} = \frac{\theta - \theta^B}{\tau}, \tag{1}$$

where θ is potential temperature horizontally averaged over the CRM domain, and θ^B is the target potential temperature. Within the boundary layer, W is linearly interpolated between its value at the top of boundary layer obtained from equation (1) and its surface value $W = 0$. Here, we simply take the boundary layer height to be 1.5 km and apply equation (1) from 1.5 km to 17 km (~100 hPa). θ^B is the observed value to which the potential temperature is relaxed at a time scale of $\tau = 4$ h. Following *Raymond and Zeng* [2005], we also place a lower bound on the value of $\frac{\partial\theta}{\partial z}$, replacing the observed value by 1 K/km if it becomes smaller than that bound.

[15] In the damped gravity wave method [*Kuang*, 2008, 2011, *Blossey et al.*, 2009, *Romps*, 2012a, 2012b], the large-scale vertical velocity is obtained using an equation that relates it to virtual temperature anomalies [see derivations in *Blossey et al.*, 2009 or *Kuang*, 2011]:

$$\frac{\partial}{\partial p}\left(\varepsilon\frac{\partial\omega}{\partial p}\right) = \frac{k^2 R_d}{p}\left(T_v - T_v^B\right), \tag{2}$$

where p is the pressure, ω is the pressure velocity, ε is the inverse of the time scale of momentum damping, k is the wave number, R_d is the dry gas constant, T_v is the domain-averaged virtual temperature, and T_v^B is the target virtual temperature against which linearized wave perturbations are defined. In idealized simulations, T_v^B is taken constant in time, while here it is set to the observed time-varying virtual temperature profile. For the experiment below, $\varepsilon = 1\ \mathrm{day}^{-1}$ and $k = 10^{-6}\ \mathrm{m}^{-1}$. The elliptic equation (2) is solved with boundary conditions $\omega = 0$ at the surface and 100 hPa. Both equations (1) and (2) are solved at every time step of the model integrations.

[16] In one set of integrations, the target potential temperature, θ^B , and virtual temperature, T_v^B, are taken from the observations directly. However, because of model biases, observational errors, or other factors, the observed time-mean state may differ from the model's own equilibrium, and this may generate biases when using equation (1) or (2) to derive W. An alternative method is to derive only the time-varying perturbations in the target potential temperature or virtual temperature from the observations and impose those perturbations on top of time-mean profiles taken from a "no large-scale circulation" integration, which is nearly identical to the reference simulations except that the large-scale vertical motion is not imposed. In other words, we may add to θ^B a "correction" term, θ^C, which equal to the difference between the time mean of the model's profile in the no large-scale circulation integration and the time mean of the observed potential temperature.

[17] While the time-mean large-scale vertical velocity did not vanish over the IFA during TOGA-COARE, we hypothesize that using the no large-scale circulation profile as a reference may reduce any bias which is due to differences between the model's natural convectively adjusted state and that observed. This hypothesis appears to be partly correct; the correction improves WTG simulations, as shown below, though it does not improve the Damped-wave simulation.

Table 1. Basic Statistics of Daily Rainfall From All the Damped-Wave Experiments Without a Correction θ^c and WTG Experiments With a Correction θ^c [a]

	Damped-Wave Experiments			WTG Experiments (With θ^c)		
	Mean/SD	Lag1	R_{xy}	Mean/SD	Lag1	R_{xy}
All forcings	9.77/10.53	0.70	0.52	8.20/8.26	0.89	0.46
Fix-winds	5.01/6.04	0.52	0.44	3.97/4.42	0.76	0.40
Fix-radiation	12.56/10.45	0.54	0.37	7.50/7.17	0.85	0.34
Fix-temperature	9.87/7.96	0.78	0.52	5.30/5.43	0.91	0.40
Fix-SST	9.57/11.08	0.73	0.41	8.50/9.07	0.91	0.39
Fix-SST-winds	4.40/5.34	0.42	0.36	3.97/4.42	0.76	0.40

[a]Columns 2, 3, and 4 are mean (mm/d) and standard deviation, lag 1 autocorrelation, and correlation coefficient with budget-derived daily rainfall for all the Damped-wave experiments. Columns 5, 6, and 7 are the same as Columns 2, 3, and 4 but for all the WTG experiments. Column 2 and 3 can be compared to budgeted-derived rainfall, which has a mean of 8.42 mm/d, standard deviation of 8.33 mm/d, and Lag 1 autocorrelation coefficient of 0.36. Correlation coefficients are all statistically significant at the 95% confidence level.

[18] The model is initialized with the sounding on 00Z 1 November 1992. We discuss multiple experiments using the above-mentioned two methods. The first one, with imposed large-scale vertical velocity, will be referred to as "Imposed-W." The experiments using the WTG and damped gravity wave methods will be referred to as "WTG" and "Damped-wave," respectively. Uniformly distributed random noise of magnitude 1 K is added to the initial potential temperature field. In the WTG simulation without the correction term, θ^C, as described above, we find that the model atmosphere settles into a persistently dry, nonprecipitating state. This behavior is presumably directly related to the existence of multiple equilibria under steady forcings [*Sobel et al.*, 2007; *Sessions et al.*, 2010]. We prevent the occurrence of this dry solution by setting the initial relative humidity to 85% over the whole troposphere, and so use this ad hoc step in the WTG simulations which do not use the correction of the time-mean temperature profile to the "zero large-scale circulation" profile.

[19] We do not compute radiative fluxes interactively in either the WTG or the Damped-wave experiments. Instead, we impose the time-dependent areal-mean radiative heating obtained from the Imposed-W experiment. We do this to avoid complications resulting from cloud-radiative feedbacks. These feedbacks are much more important with parameterized dynamics than in the standard approach and can cause large errors. We leave the detailed investigation of the role of radiation to future work and specify the radiative heating in the parameterized dynamics experiments in order to better control them. In all experiments, we specify the SST and relax the horizontal mean profile of horizontal wind toward that observed.

[20] In both sets of simulations, observations influence the model through four pathways: the zonal and meridional winds, the model-derived radiation from the Imposed-W experiment (in which the convection is closely constrained by the imposed vertical motion, and the clouds and water vapor strongly influence the radiation), the observed SST, and the free-tropospheric temperature. The first three forcings are directly related to moist static energy sources; surface winds and SST control the surface turbulent fluxes, and radiation is a direct forcing on moist static energy. The free-tropospheric temperature, on the other hand, is a state variable and can influence the moist static energy budget only indirectly through its coupling with large-scale vertical motion and the other interactive processes.

[21] To further clarify the relative importance of the four forcing factors to the model-simulated surface rainfall, sensitivity experiments are performed in which we replace one time-dependent forcing at a time with its time-mean value. These experiments are named Fix-winds, Fix-radiation, Fix-SST, and Fix-temperature, respectively. Fix-wind and Fix-SST both reduce variability in surface turbulent fluxes; to further examine the role of these fluxes, another experiment (named Fix-SST-winds) is also performed in which both are replaced by time-mean values. All these experiments are done using both the Damped-wave and WTG methods.

3. Results

3.1. Damped-Wave and WTG Experiments

[22] Figure 1a shows the domain-averaged rainfall from the Imposed-W experiment. COARE budget-derived rainfall

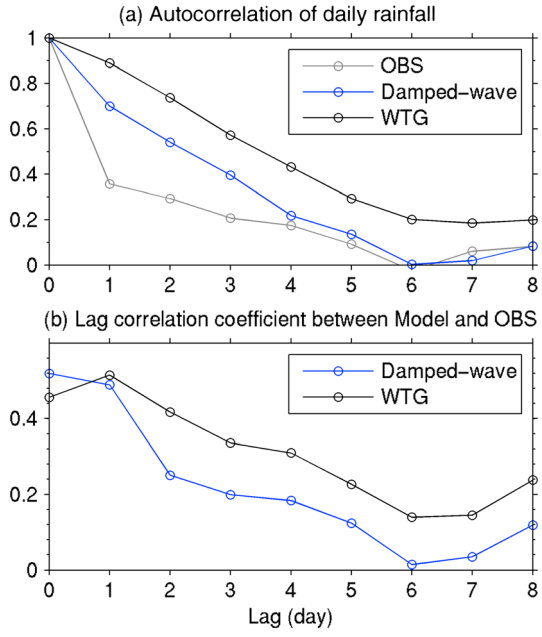

Figure 2. (a) Autocorrelation of daily rainfall from observation (gray), the Damped-wave (blue, Figure 1d), and WTG (black, Figure 1c) experiments. (b) Lagged correlation coefficient of daily rainfall between observation and model results for the Damped-wave (blue) and the WTG (gray) experiments. Positive lag in Figure 2b means the model lags the observations.

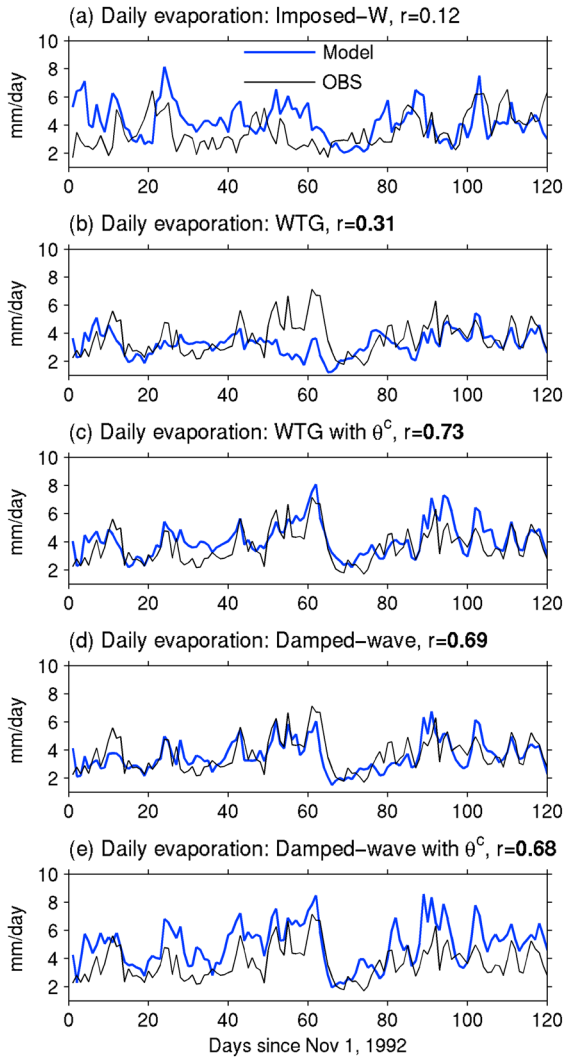

Figure 3. Daily mean surface evaporation from COARE (black curves) and model simulations (blue) for (a) the Imposed-W experiment, (b) the WTG experiment, (c) as Figure 3b but with a correction θ^c to the target temperature profile (d) the Damped-wave experiment, and (e) as Figure 3d but with θ^c.

is also shown in black. Rainfall from the Imposed-W simulation shows good agreement with the COARE budget-derived rainfall, as expected.

[23] The domain-averaged rainfall time series from the WTG and Damped-wave experiments are shown in Figures 1b and 1c and Figures 1d and 1e. Figures 1b and 1d show results in which target (potential/virtual) temperature profiles are directly from large-scale forcing data set, while in Figures 1c and 1e target (potential/virtual) temperature profiles are modified using the correction term described above so that the time-mean profile is equal to that from a reference simulation with zero large-scale circulation. Comparison between Figures 1b and 1c and Figures 1d and 1e indicates that this correction improves the results obtained with the WTG method, but not those obtained with the Damped-wave method. In the following, we will present the results from the WTG experiment with the correction term but without it in the Damped-wave experiment.

[24] The rainfall simulated with parameterized large-scale dynamics, using either method, does not agree with the budget-derived rainfall from the observations as well as that from the Imposed-W experiment does. This is also as expected. The large-scale vertical velocity—which controls the dominant terms in the heat and moisture equations as shown in Figure 1a—is no longer taken from observations. It is now a nontrivial part of the solution, depending on the validity of the large-scale parameterization using equation (1) or (2), as well as on model physics and other choices (numerics, resolution, domain size, etc.), and is free to deviate from that observed. It is not obvious, a priori, that the simulation need capture the observed variability of precipitation at all. There is, however, some agreement, particularly on the intraseasonal time scale. These experiments (Figures 1c and 1d) capture the convectively suppressed period during days 15–30, the convectively active phase of the first MJO event during days 35–55, and, to a lesser (but still significant) extent, the second MJO event for the last 20 days. Significant deviations from observations are also evident. Both simulations produce too little rainfall during days 65–80 and overestimate rainfall during days 90–100. The WTG experiment without the correction to the time-mean potential temperature profile has an extended strong rainy phase that was not observed during days 50–70. The Damped-wave experiment shows good agreement with the observations during this period but simulates too little rainfall during the first 15 days.

[25] Some basic statistics of surface rainfall from the WTG and Damped-wave experiments are shown in the second row of Table 1. The mean and standard deviation are 9.77 mm/d and 10.53 mm/d, respectively, for Damped-wave; and 8.20 mm/d and 8.26 mm/d, respectively, for WTG. These values can be compared to those from the budget-derived rainfall, 8.42 mm/d and 8.33 mm/d. The 1 day lag autocorrelation coefficient of the surface rainfall time series is 0.70 for Damped-wave and 0.89 for WTG, higher in both cases than that derived from observations (0.36). These autocorrelation coefficients influence the number of independent samples assumed in statistical significance calculations.

[26] Figure 2b shows the lag correlation coefficient between the model-simulated and budget-derived daily rainfall. The lag 0 value is 0.46 for WTG and 0.52 for Damped-wave. The statistical significance of these correlations is tested using the standard T test, with the degrees of freedom adjusted by the lag autocorrelation coefficients as *Livezey and Chen* [1983]. The correlation coefficient of 0.52 in Damped-wave and 0.46 in WTG are both significant at 95% level. The correlation coefficient is actually slightly greater at lag 1 than at lag 0 in WTG and has a broad maximum over days 1 and 2 (close to 0.5) in both simulations. These values again are statistically significant using the autocorrelation from the simulation.

[27] Figure 3 compares the domain-averaged surface evaporation with observations. Interestingly, the simulated surface evaporation agrees significantly better in the Damped-wave experiment than in the Imposed-W experiment. We do not have a good explanation for this at present, but simply note that we expect surface flux errors to have a lesser influence on precipitation in the Imposed-W case than in the parameterized W cases. Moisture convergence provides most of the moisture for precipitation, and it is specified

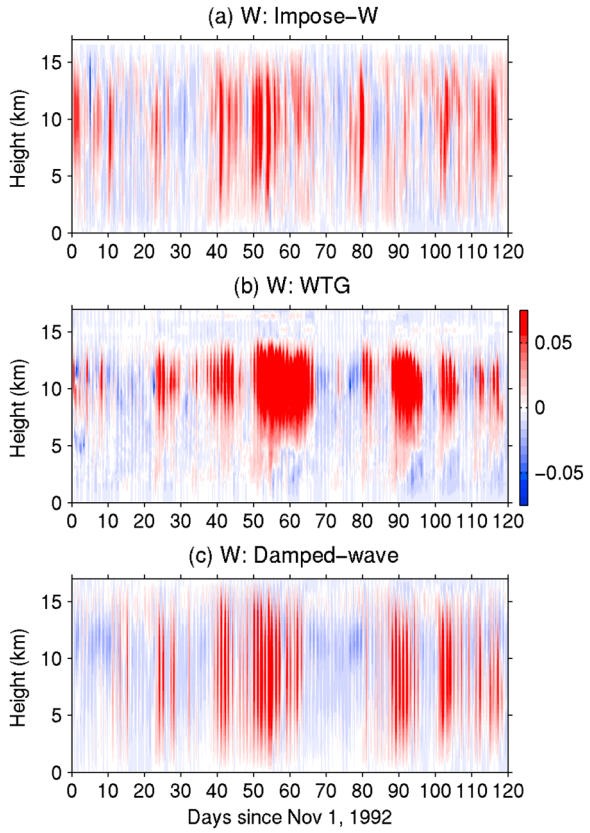

Figure 4. Large-scale vertical motion as a function of time and height for (a) the observations (and Imposed-W experiment), (b) the WTG experiment, and (c) the Damped-wave experiment.

(approximately; it does depend on the simulated moisture profile, but its time variations are strongly controlled by those in the large-scale vertical velocity) in the Imposed-W experiment while it is a result of the other forcings, including the surface fluxes and radiation, in the cases with parameterized W.

[28] Figure 4 shows the large-scale vertical motion as a function of time and height from OBS and from the WTG and Damped-wave simulations. In both, the degree of agreement in the time variability is similar to that in precipitation. However, we see extended strong ascent during active phases in WTG, and some additional high-frequency variability in the Damped-wave experiment. Figure 5 compares the time-averaged vertical profiles of large-scale vertical velocity. While there is good agreement in the lower troposphere between model and OBS, the shapes of the parameterized large-scale W profiles deviate from OBS significantly. The profile from WTG is too top-heavy, with a peak value more than 30 cm/s around 11 km, as opposed to ~15 cm/s in observations, while the Damped-wave simulation is insufficiently top-heavy, with a peak around 7 km, as opposed to ~12 km in observations.

[29] We can understand this difference between the two methods qualitatively. The relaxation time scale τ in equation (1) and the combination of wave number and momentum damping, k^2/ε, in equation (2) are key parameters linking temperature anomalies and large-scale vertical motions in these two methods. In WTG, the coupling between temperature anomalies and WTG vertical motion occurs on the WTG time scale, which is the same for all vertical modes, because the relationship between temperature anomalies and vertical motion anomalies, (1), is strictly local in the vertical. The Damped-wave method incorporates a momentum budget and hydrostatic balance and involves an elliptic problem in which the response of W to T_v is nonlocal in the vertical (equation (2)). Upper-level temperature anomalies, for example, can influence the circulation at lower levels. Arguments as to why this nonlocality should result specifically in less top-heavy profiles in particular are discussed in [*Kuang*, 2011, 2012]: in the Damped gravity wave approach, for the different vertical modes, temperature anomalies required to sustain vertical motion of a given amplitude are proportional to the inverse of their gravity wave phase speed and are therefore higher for higher vertical modes. At the same time, the temperature anomalies are also constrained by the convective tendencies that they incur. As a result, higher vertical modes are suppressed relative to the gravest mode. The gravest mode peaks in the middle troposphere, thus the fact that it is favored leads to less top-heavy profiles.

[30] In the Damped-wave method, we also expect the shape of the vertical motion profile to be influenced by the value and vertical structure of the Rayleigh drag coefficient, ε, (here taken constant) in equation (1). The sensitivity to this quantity and to the form of the damping (which need not be formulated as a Rayleigh drag [see, e.g., *Kuang*, 2011]) will be explored in future work.

3.2. Sensitivity Experiments

[31] The simulated surface rainfall and evaporation from all the Damped-wave sensitivity experiments are shown in the left columns of Figures 6 and 7, respectively; the WTG sensitivity experiments are shown in

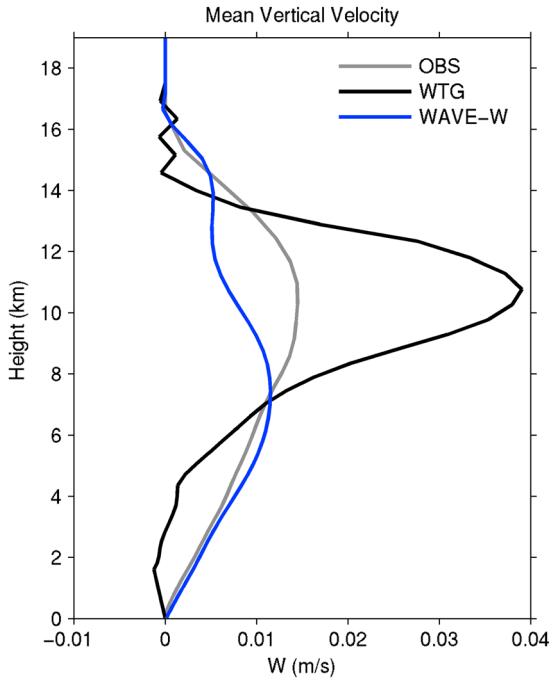

Figure 5. Time-averaged vertical velocity profiles from COARE (gray), the WTG experiment (black), and the Damped-wave experiment (blue).

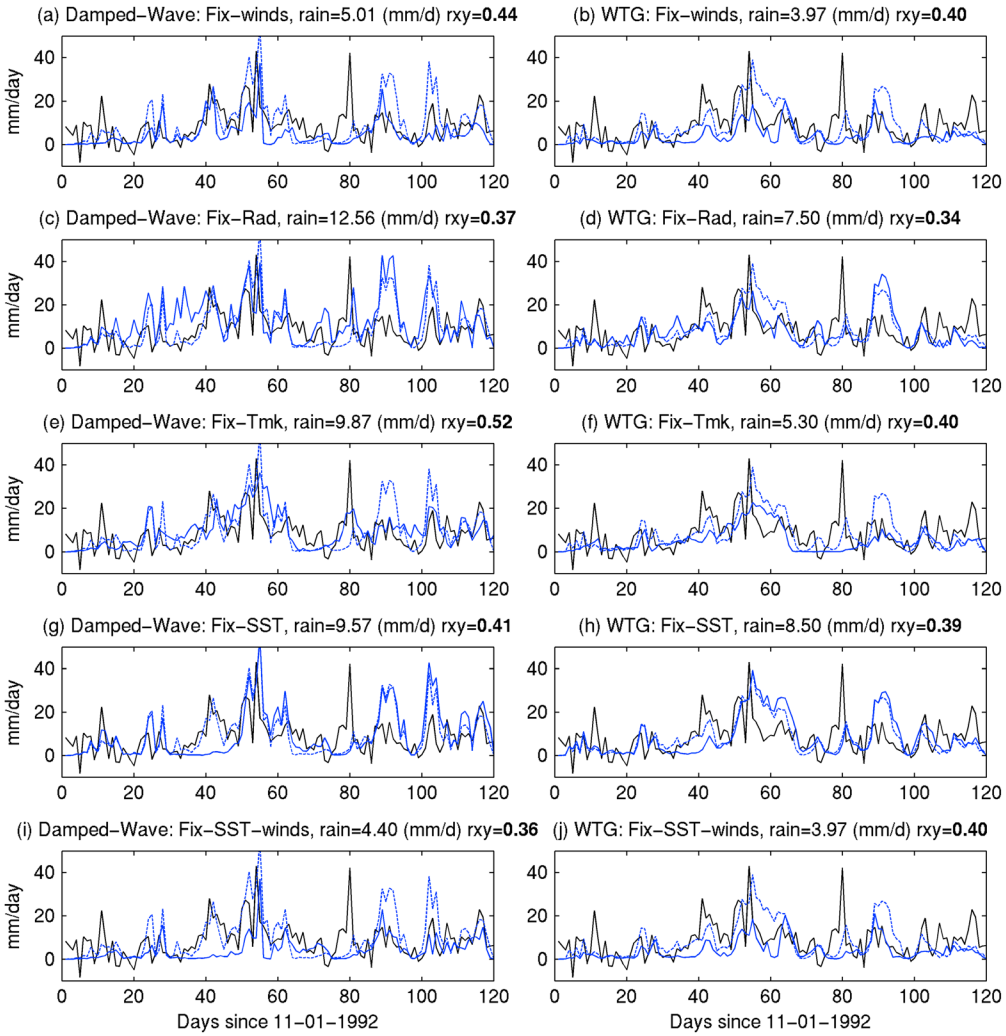

Figure 6. Daily rainfall from the experiments in which one time-varying forcing at a time is replaced by its time mean. Blue and black curves denote model results and budget-derived rain rate. Dashed curves indicate the full simulations shown in Figures 1c and 1d. (left) Damped-wave sensitivity experiments with winds, radiation, free tropospheric temperature, SST, and both SST and winds replaced by their time-mean values, respectively. (right) Same as in the left column but for WTG experiments. Bold values of correlation coefficient, *r*, indicate that it is statistically significant at the 95% level.

the right columns of the same figures. Basic statistics of rainfall are also shown in Table 1. We first discuss the Damped-wave sensitivity experiments.

[32] In Figures 6a and 7a, in which surface winds are set to their time-mean value, the time means of both surface evaporation and rainfall are strongly reduced; the mean precipitation is reduced to 5.01 mm/d. The standard deviation of precipitation is also reduced to 6.04 mm/d. Despite the constant surface wind speed, some variability in surface evaporation still occurs; for example, evaporation is high during days 25–45. This is due to high SST, as can be seen from the Fix-SST experiment (Figures 6g and 7g), in which using time-mean SST leads to reductions in evaporation and rainfall during days 25–45. The role of surface turbulent fluxes overall can be assessed from the Fix-SST-winds experiment (Figures 6i and 7i), in which the mean and standard deviation of rainfall are 4.40 mm/d and 5.34 mm/d, respectively, and the correlation coefficient of the simulated and observed daily precipitation is reduced to 0.36.

[33] The importance of time-varying radiation can be seen in the Fix-radiation experiment (Figures 6c and 7c), in which the mean and standard deviation of rainfall are 12.56 mm/d and 10.45 mm/d, respectively; and the correlation coefficient with observed daily precipitation is reduced to 0.37, nearly the same as that in Fix-SST-winds. These reductions in the rainfall correlation coefficient suggest that variations in both surface turbulent fluxes and radiative cooling are important to the model-simulated rainfall variability.

[34] On the other hand, setting the reference-free tropospheric temperature profile to its time-mean value has no impact; the simulated rainfall's correlation coefficient with the observed one is almost the same (0.52). It should be kept in mind that the horizontal mean temperature profile itself is not time-independent in this simulation; the perturbations are computed interactively from (2). It is just the reference profile against which perturbations are computed that is constant. This result seems to indicate that the temperature perturbations may be better thought of as

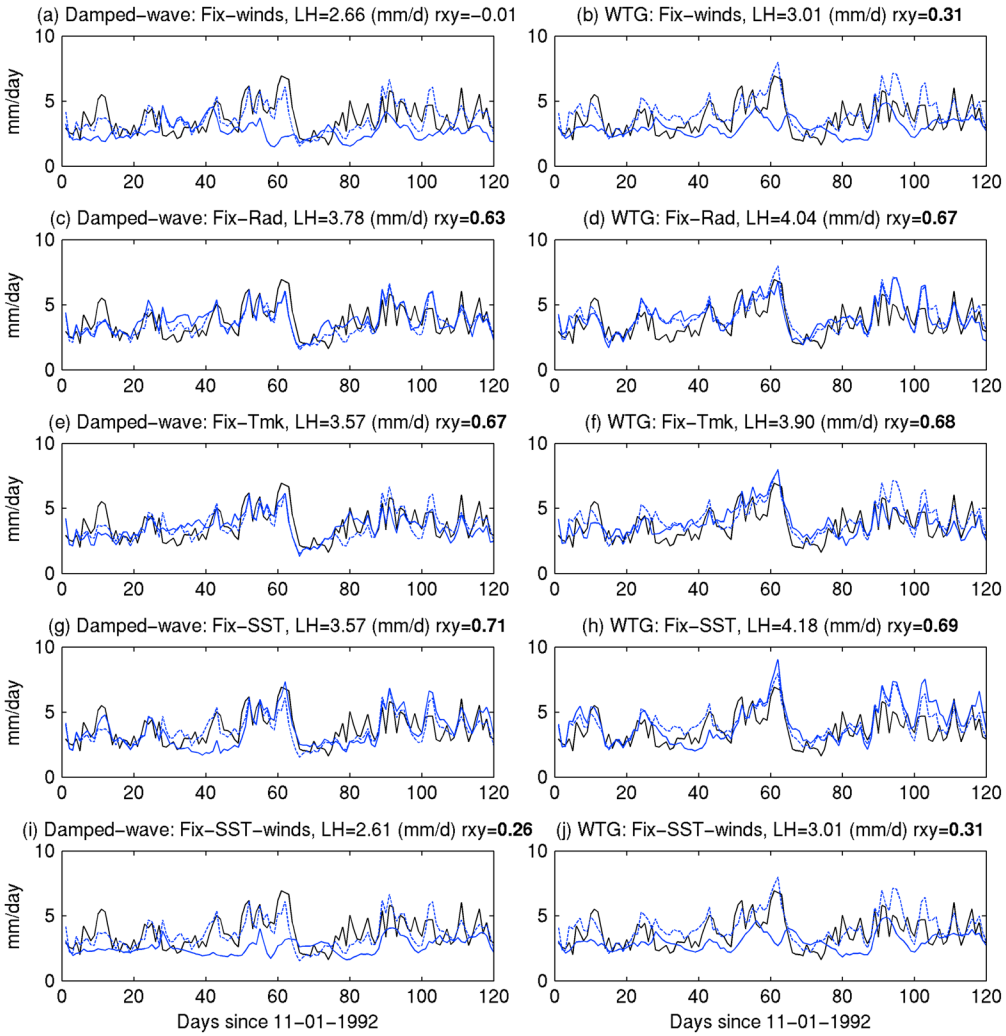

Figure 7. The same as Figure 6 but for surface evaporation. Dashed curves indicate the full simulations shown in Figures 3c and 3d.

a local response to convection rather than as consequences of external disturbances.

[35] In the WTG sensitivity experiments, the use of time-mean winds reduces the time-mean rainfall substantially (to 3.97 mm/d); its correlation with budget-derived rainfall decreases from 0.46 to 0.40 (Figure 6b). Using time-mean radiative heating also leads to a decrease in both the time-mean rainfall and the correlation of the rainfall time series with that observed; the correlation coefficient (0.34) is very close to that in the Damped-wave setting with fixed radiative heating (0.37). However, compared to the Damped-wave method, WTG is more sensitive to free-tropospheric temperature. Figure 6f indicates that using its time-mean value reduces both the time-mean rainfall (5.30 mm/d) and the correlation of the rainfall time series with that observed (0.40).

3.3. Sensitivities to Parameters in WTG and Damped-Wave Methods

[36] The relaxation time scale τ in equation (1) and wave number k in equation (2) are parameters in the two methods. Smaller τ or larger k (with a fixed value of ε) results in stronger coupling between temperature and large-scale vertical motion, while larger τ or smaller k indicates weaker coupling. While this much is straightforward, the influence of these parameters on rainfall is somewhat less so. To explore this, we vary τ and k, using the values 2, 4, 8, 12, and 24 h for τ, and 0.5×10^{-6}, 0.75×10^{-6}, 1×10^{-6}, 1.5×10^{-6}, and $3 \times 10^{-6}\,\mathrm{m}^{-1}$ for k (with $\varepsilon = 1\,\mathrm{day}^{-1}$).

[37] Figure 8 shows rainfall time series from the Damped-wave method. The daily time series are shown on the left, while 6-hourly time series are shown on the right to make the higher frequencies visible. The smallest k (0.5×10^{-6} m^{-1}) produces the smallest mean rainfall (5.37 mm/d) as expected, among the range values of k being explored, and a statistically insignificant correlation coefficient with the observed time series, 0.22. We may rationalize this based on equation (2): as k approaches zero, temperature anomalies are increasingly decoupled from vertical motion and thus rainfall. On the other hand, infinite k represents the limit of strict convective equilibrium; W responds to temperature anomalies instantly and strongly so as to eliminate them and can produce a large amount of precipitation in a short period of time, thus leading to sharp spikes in the 6-hourly rainfall time series (Figures 8h and 8j). As k is increased beyond 0.75×10^{-6} to $3 \times 10^{-6}\,\mathrm{m}^{-1}$, the mean rainfall decreases slightly, remaining close to constant at a value

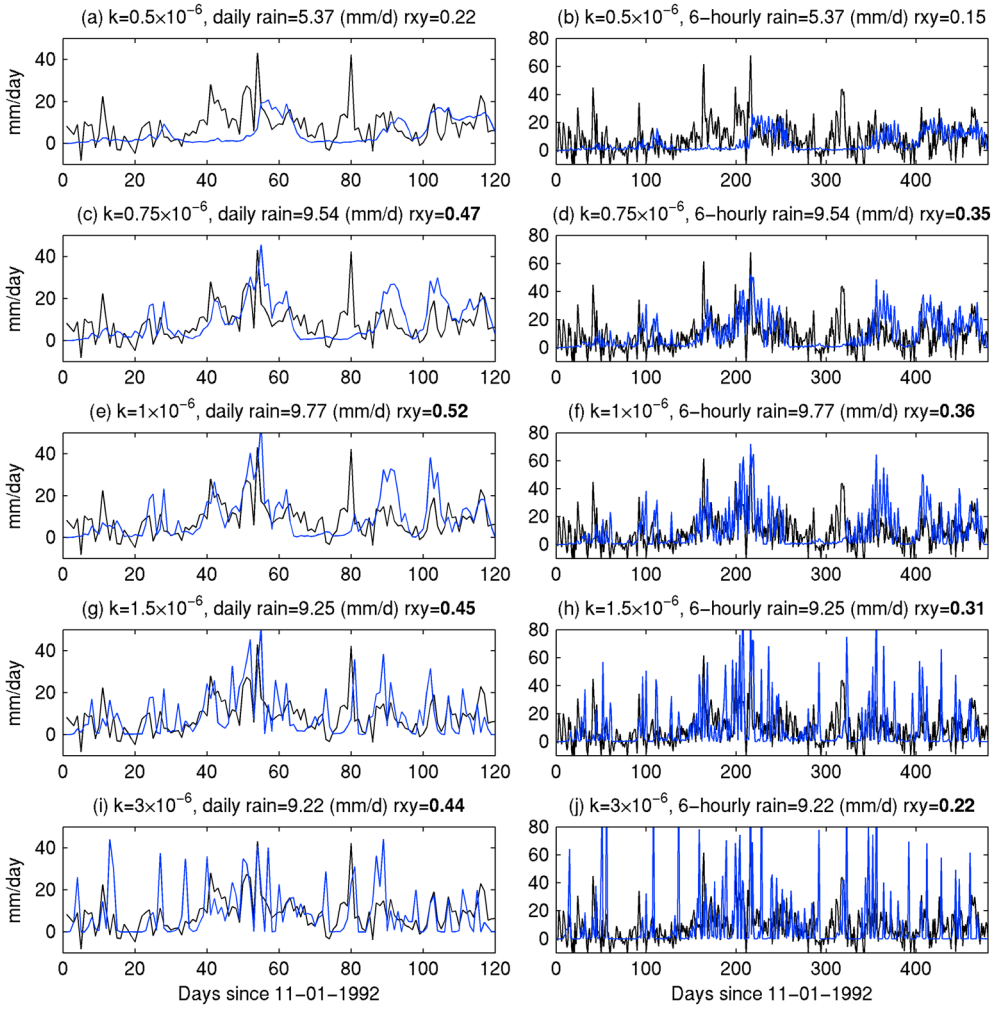

Figure 8. Sensitivity to the wave number k in equation (2) for the Damped-wave experiments. (left) Daily rainfall. (right) 6-Hourly rainfall. Mean rainfall and correlation coefficient between model-simulated rainfall and budget-derived value are also indicated in the title of each panel. Note that bold values of correlation coefficient, r, indicate that it is statistically significant at the 95% level.

slightly larger than the budget derived time-mean rainfall. Another interesting feature is the strong rainfall maximum around day 80 for $k = 1.5 \times 10^{-6}$ and $3 \times 10^{-6}\,\mathrm{m}^{-1}$ (Figures 8g and 8i), which is similar to that in the budget-derived time series but is absent for smaller k.

[38] Figure 9 shows analogous results from varying τ in WTG. As τ is decreased from 24 h to 2 h, the correlation coefficient increases from 0.15 to 0.46. The time-mean rainfall is smallest (3.93 mm/d) at largest $\tau = 24$ h, and maximizes at $\tau = 8$ h with 10.29 mm/d. The daily mean rain rate agrees best with the TOGA-COARE value at $\tau = 4$ h (8.20 mm/d).

[39] The non-monotonic behavior with increasing τ or decreasing k was found in idealized simulations with time-independent forcings by *Wang and Sobel* [2011] and *Kuang* [2011, 2012]. At small τ or large k, increases in τ or decreases in k allow greater upper-tropospheric warming and static stability. This causes a shallowing of the large-scale vertical motion profile and a decrease in the gross moist stability, thus increasing rainfall. At sufficiently large τ or small k, however, the large-scale vertical motion must become small, since the large-scale vertical motion is proportional to $1/\tau$ under WTG, or k^2 in the Damped-wave method. For these simulations in which the large-scale vertical motion is otherwise upward in the mean, this implies a reduction in moisture convergence and thus precipitation.

4. Discussion and Conclusions

[40] In this study, the variability of deep convection during the 4-month TOGA-COARE field program is simulated using a cloud-resolving model with large-scale dynamics parameterized using two different methods: the weak temperature gradient method and the Damped gravity wave method. The results are compared to the observations, with a focus on the time series of area-averaged precipitation, and to the results from a more standard simulation in which the large-scale vertical motion is prescribed.

[41] The simulations with parameterized large-scale dynamics, though far from perfect, are able to simulate the intraseasonal variability of surface rainfall with some success. The vertical profile of parameterized large-scale vertical motion is too top-heavy using the WTG method and insufficiently top-heavy using damped gravity wave method as compared to observations, though we expect this to be sensitive to the treatment of momentum damping in the latter.

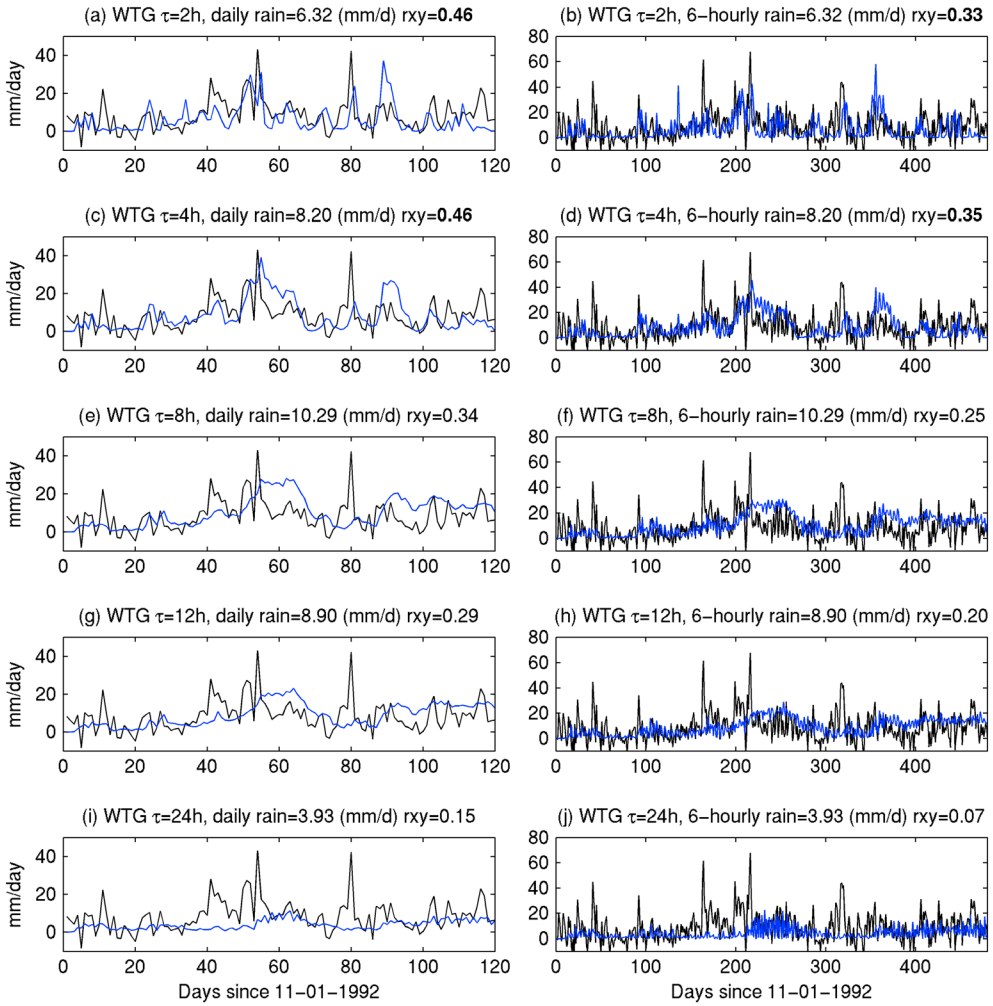

Figure 9. Sensitivity to time scale $\tau = 2$, 4, 8, 12, and 24 h in the WTG experiments. (left) Daily rainfall. (right) 6-Hourly rainfall. Mean rainfall and correlation coefficient between model-simulated rainfall and budget-derived value. Note that bold values of correlation coefficient, *r*, indicate that it is statistically significant at the 95% level.

[42] Sensitivity experiments are performed to assess the relative importance of the different factors imposed from observations to the model-simulated rainfall variability. In both the Damped-wave and WTG experiments, surface turbulent fluxes and radiation both contribute strongly to simulated rainfall variability, although their relative importance differs in the two methods. However, these two methods show very different sensitivity to time-variations in the reference free tropospheric virtual temperature profile: the Damped-wave method shows no impact, while the WTG method is more sensitive to this, with less agreement in surface rainfall and surface fluxes.

[43] To explore the impact of changes in the key parameters in the two methods, the relaxation time scale τ and wave number k, numerical experiments are performed with a range of parameter values. Surface rainfall is the smallest in both methods for the weakest coupling between temperature anomalies and large-scale vertical motion. A local precipitation maximum exists in the parameter space of τ for WTG, while precipitation in the Damped-wave experiments level off with large k. This non-monotonic behavior is similar to that found in previous studies which analyzed idealized experiments.

[44] Those factors which directly influence the forcing of the column-integrated moist static energy budget—surface winds and SST (through surface turbulent fluxes) and radiative cooling—have a greater influence than the one factor, free-tropospheric temperature, which is a state variable and can influence the moist static energy budget only indirectly. This is particularly true with the damped gravity wave method. This lends some support to theories of MJO dynamics which focus on the moist static energy budget in general and surface fluxes and radiation in particular [e.g., *Raymond*, 2001; *Sobel et al.*, 2008, 2010; *Sobel and Maloney*, 2012, 2013].

[45] More broadly, these results encourage us to think that simulations with interactive large-scale dynamics may provide a new and useful modality for comparing CRMs and single-column models to observations from field campaigns. A number of issues need to be explored in more depth first, however, in order for us to understand the strengths and limitations of the methods. Important issues include the roles of interactive radiation, horizontal advection of moisture, mesoscale convective organization (which may depend on domain size), and

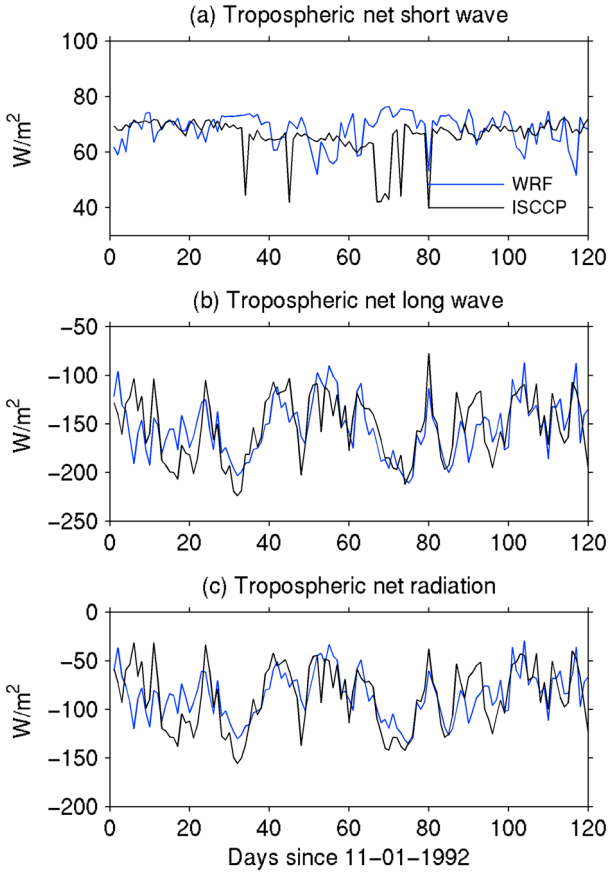

Figure A1. Net tropospheric radiative heating from the Imposed-W experiment and from the ISCCP data set. (a) Daily mean of net short wave heating, (b) net long wave heating, and (c) net radiative heating.

initial conditions. Study of these issues is underway and will be reported in due time.

Appendix A: CRM-Simulated Radiative Heating

[46] In Appendix A, we compare radiative heating from the Imposed-W experiment against the ISCCP (International Satellite Cloud Climatology Project) FDX data set [*Rossow and Zhang*, 1995]. Figure A1 shows daily mean tropospheric radiative heating (integrated over the troposphere), including short-wave, long-wave, and the net tropospheric heating, from the Imposed-W experiment and from the ISCCP data set. Except for the first 10 days, model-simulated radiative fluxes agree with ISCCP quite well in both time variability and time mean. Daily mean net tropospheric radiative heating is -87.6 W/m^2 from the ISCCP and -85.8 W/m^2 from the model.

[47] **Acknowledgments.** This work was supported by NSF grants AGS-1062206 and AGS-1008847. We thank NCAR's Computational and Information Systems Laboratory, where the numerical experiments were performed. We thank Sharon Sessions and David J. Raymond for the discussions. We also thank David J. Raymond and Sandrine Bony for their constructive comments.

References

Bergman, J., and P. D. Sardeshmukh (2004), Dynamic stabilization of atmospheric single column models, *J. Clim.*, *17*, 1004–1021.

Blossey, P. N., C. S. Bretherton, J. Cetrone, and M. Khairoutdinov (2007), Cloud-resolving model simulations of KWAJEX: Model sensitivities and comparisons with satellite and radar observations, *J. Atmos. Sci.*, *64*, 1488–1508.

Blossey, P. N., C. S. Bretherton, and M. C. Wyant (2009), Subtropical low cloud response to a warmer climate in an superparameterized climate model. Part II: Column modeling with a cloud resolving model, *J. Adv. Model. Earth Syst.*, *1*, Art. #8, 14 pp., doi:10.3894/JAMES.2009.1.8

Chen, S. S., R. A. Houze, Jr., and B. E. Mapes (1996), Multiscale variability of deep convection in relation to large-scale circulation in TOGA COARE, *J. Atmos. Sci.*, *53*, 1380–1409.

Ciesielski, P. E., R. H. Johnson, P. T. Haertel, and J. Wang (2003), Corrected TOGA COARE sounding humidity data: Impact on diagnosed properties of convection and climate over the warm pool, *J. Clim.*, *16*, 2370–2384.

Collins, W. D., et al. (2004), Description of the NCAR Community Atmosphere Model (CAM3.0), *NCAR Tech. Note, NCAR/TN-464+STR, 226* pp., Natl. Cent. for Atmos. Res., Boulder, Colo.

Emanuel, K. A., and M. Živković-Rothman (1999), Development and evaluation of a convection scheme for use in climate models, *J. Atmos. Sci.*, *56*, 1766–1782.

Fridlind, A. M., et al. (2012), A comparison of TWP-ICE observational data with cloud-resolving model results, *J. Geophys. Res.*, *117*, D05204, doi:10.1029/2011JD016595.

Grabowski, W. W., X. Wu, and M. W. Moncrieff (1996), Cloud resolving modeling of tropical cloud systems during phase III of GATE: I. Two-dimensional experiments, *J. Atmos. Sci.*, *53*, 3684–3709.

Hong, S.-Y., Y. Noh, and J. Dudhia (2006), A new vertical diffusion package with an explicit treatment of entrainment processes, *Mon. Weather Rev.*, *134*, 2318–2341.

Johnson, D. E., W.-K. Tao, J. Simpson, and C.-H. Sui (2002), A study of the response of deep tropical clouds to large-scale thermodynamic forcings: I. Modeling strategies and simulations of TOGA COARE convective systems, *J. Atmos. Sci.*, *59*, 3492–3518.

Khairoutdinov, M. F., and D. A. Randall (2003), Cloud resolving modeling of the ARM Summer 1997 IOP: Model formulation, results, uncertainties, and sensitivities, *J. Atmos. Sci.*, *60*, 607–625.

Klemp, J. B., J. Dudhia, and A. D. Hassiotis (2008), An upper gravity-wave absorbing layer for NWP applications, *Mon. Weather Rev.*, *136*, 3987–4004.

Kuang, Z. (2008), Modeling the interaction between cumulus convection and linear gravity waves using a limited-domain cloud system-resolving model, *J. Atmos. Sci.*, *65*, 576–591.

Kuang, Z. (2011), The wavelength dependence of the gross moist stability and the scale selection in the instability of column integrated moist static energy, *J. Atmos. Sci.*, *68*, 61–74.

Kuang, Z. (2012), Weakly forced mock-Walker cells, *J. Atmos. Sci. 69*, 2759–2786.

Lin, Y.-L., R. D. Farley, and H. D. Orville (1983), Bulk parameterization of the snow field in a cloud model, *J. Clim. Appl. Meteorol.*, *22*, 1065–1092.

Livezey, R. E., and W. Y. Chen (1983), Statistical field significance and its determination by Monte Carlo techniques. *Mon. Weather Rev.*, *111*, 46–59.

Mapes, B. E. (1997), What controls large-scale variations of deep convection? in *New Insights and Approaches to Cumulus Parameterization, ECMWF Workshop Proceedings, Reading, U.K., November 1996*, pp. 157–165.

Mapes, B. E. (2004), Sensitivities of cumulus ensemble rainfall in a cloud-resolving model with parameterized large-scale dynamics, *J. Atmos. Sci.*, *61*, 2308–2317.

Raymond, D. J. (2001), A new model of the Madden-Julian oscillation, *J. Atmos. Sci.*, *58*, 2807–2819.

Raymond, D. J., and S. L. Sessions (2007), Evolution of convection during tropical cyclogenesis, *Geophys. Res. Lett.*, *34*, L06811, doi:10.1029/2006GL028607.

Raymond, D. J., and X. Zeng (2005), Modelling tropical atmospheric convection in the context of the weak temperature gradient approximation, *Q. J. R. Meteorol. Soc.*, *131*, 1301–1320

Romps, D. (2012a), Numerical tests of the weak pressure gradient approximation, *J. Atmos. Sci.*, *69*, 2846–2856.

Romps, D. (2012b), Weak pressure gradient approximation and its analytical solutions, *J. Atmos. Sci.*, *69*, 2835–2845.

Rossow, W. B., and Y.-C. Zhang (1995), Calculation of surface and top of atmosphere radiative fluxes from physical quantities based on ISCCP data sets: 2. Validation and first results, *J. Geophys. Res.*, *100*, 1167–1197.

Sessions, S., D. J. Raymond, and A. H. Sobel (2010), Multiple equilibria in a cloud-resolving model, *J. Geophys. Res.*, *115*, D12110, doi:10.1029/2009JD013376.

Skamarock, W. C., J. B. Klemp, J. Dudhia, D. O. Gill, D. M. Barker, M. G. Duda, X. Huang, W. Wang, and J. G. Powers (2008), A description of the advanced research WRF version 3, *NCAR Tech. Note NCAR/TN–475+STR*, 125 pp, Natl. Cent. for Atmos. Res., Boulder, Colo.

Sobel, A. H., and G. Bellon (2009), The effect of imposed drying on parameterized deep convection, *J. Atmos. Sci.*, *66*, 2085–2096.

Sobel, A. H., and C. S. Bretherton (2000), Modeling tropical precipitation in a single column, *J. Clim.*, *13*, 4378–4392.

Sobel, A. H., and E. D. Maloney (2012), An idealized semi-empirical framework for modeling the Madden-Julian oscillation, *J. Atmos. Sci.*, *69*, 1691–1705.

Sobel, A. H., and E. D. Maloney (2013), Moisture modes and the eastward propagation of the MJO, *J. Atmos. Sci.*, in press.

Sobel, A. H., G. Bellon, and J. Bacmeister (2007), Multiple equilibria in a single-column model of the tropical atmosphere, *Geophys. Res. Lett.*, *34*, L22804, doi:10.1029/2007GL031320.

Sobel, A. H., E. D. Maloney, G. Bellon, and D. M. W. Frierson (2008) The role of surface fluxes in tropical intraseasonal oscillations, *Nat. Geosci.*, *1*, 653–657.

Sobel, A. H., E. D. Maloney, G. Bellon, and D. M. W. Frierson (2010), Surface fluxes and tropical intraseasonal variability: A reassessment, *J. Adv. Model. Earth Syst.*, *2*, doi:10.3894/JAMES.2010.2.2.

Soong, S.-T., and Y. Ogura (1980), Response of tradewind cumuli to large-scale processes, *J. Atmos. Sci.*, *37*, 2035–2050.

Tao, W.-K., D. Johnson, C.-L. Shie, and J. Simpson (2004), The atmospheric energy budget and large-scale precipitation efficiency of convective systems during TOGA COARE, GATE, SCSMEX, and ARM: Cloud-resolving model simulations, *J. Atmos. Sci.*, *61*, 2405–2423.

Wang, S., and A. H. Sobel (2011), Response of convection to relative sea surface temperature: Cloud-resolving simulations in two and three dimensions, *J. Geophys. Res.*, *116*, D11119, doi:10.1029/2010JD015347.

Wang, S., and A. H. Sobel (2012), Impact of imposed drying on deep convection in a cloud-resolving model, *J. Geophys. Res.*, *117*, D02112, doi:10.1029/2011JD016847.

Webster, P. J., and R. Lukas (1992), TOGA COARE: The coupled ocean-atmosphere response experiment, *Bull. Am. Meteorol. Soc.*, *73*, 1377–1416.

Wu, X., W. W. Grabowski, and M. W. Moncrieff (1998), Long-term behavior of cloud systems in TOGA COARE and their interactions with radiative and surface processes: I. Two-dimensional modeling study, *J. Atmos. Sci.*, *55*, 2693–2714.